



Structure and reversible crystal-to-crystal transformations of a zinc(II) coordination polymer constructed from an imide-based dicarboxylic acid



Chung-Yu Chang, Meng-Jung Tsai, Jing-Yun Wu *

Department of Applied Chemistry, National Chi Nan University, Nantou, 545, Taiwan

ARTICLE INFO

Keywords:

Coordination polymer
Crystal-to-crystal transformation
Helical chain
Zinc

ABSTRACT

An imide-based O-donor ligand, 4-carboxyphenyl-1,3-dioxoisindoline-5-carboxylic acid ($H_2In\text{-}4\text{-ba}$), and one Zn(II) coordination polymer, $[Zn(In\text{-}4\text{-ba})(py)_2]_n$ (**1**, py = pyridine), have been synthesized. Single-crystal X-ray diffraction indicates that **1** has a quasi- 3_1 helical chain structure, which shows one-dimensional to two-dimensional (1D → 2D) extension to be a homochiral layer of consecutively interweaving poly-helices with the same helicity. Coexistence of such homochiral layers in opposite chirality makes individual crystal of **1** to be in a racemic manner. Thermogravimetric (TG) analysis indicated that **1** shows high thermal stability approaching 440 °C. Thermal activation of **1** gives a desolvated phase, $[Zn(In\text{-}4\text{-ba})]_n$ (**1'**), as supported by TG trace. Of particular note, reversible crystal-to-crystal transformations between solvated **1** and desolvated **1'** have been achieved upon decoordination and recoordination of the py ligands, as evidenced by XRPD patterns, IR spectra, and TG diagrams. The photoluminescence properties of as-synthesized **1**, desolvated **1'**, and resolvated **1'/py** have also been studied. All of them exhibit an emission band centered at 486, 492, and 486 nm, respectively, which is originated from the ligand-centered charge transfer. Further, the emission intensity of **1'** is weaker than that of **1** and **1'/py**, implying the influence of coordinated py ligands and/or structure regulation on photoluminescence.

1. Introduction

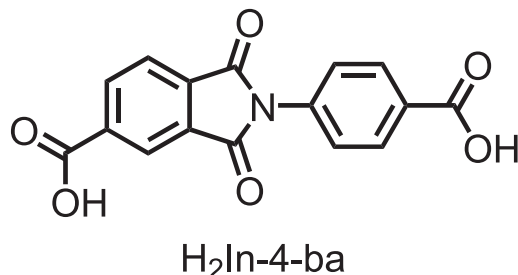
Coordination polymers with infinite multi-dimensional periodical net structure of metal ions/clusters connected by organic linkers have attracted a great deal of interest in the past decades due to their fascinating structure characteristics of many kinds of net topologies and multiple functionalities in gas sorption, catalysis, chemical sensing, energy storage and conversion, and so on [1–14]. From a structural point of view, one fascinating discovery is the stimuli-responsive structural flexibility, which results in solid-state structural transformations [15–18]. Up to now, several driving forces involving external chemical stimuli, such as solvent exclusion [19–23], solvent exchange [23–25], and ion exchange [26–28], and external physical stimuli, such as heat [20,29,30], light [31,32], and mechanochemical force [30,33] have been found to trigger the occurrence of solid-state structural transformations. On the other hand, there are several types of reversible or irreversible structural transformations, such as single-crystal to single-crystal transformation showing the maintenance of single-crystal character [23–27,30–32], crystal-to-crystal transformation showing the loss of single-crystal character but retention of crystallinity [19,28,29,33], crystal-to-amorphous

transformation showing the collapse of crystallinity [20–22]. Of particular note, solid-state structural transformations demonstrate not only remarkable framework conversion but also the change of physical properties [21,29–31].

Our group is interesting in this field, and has reported several cases that show reversible one-dimensional to two-dimensional (1D-to-2D) single-crystal to single-crystal (SCSC) transformation [34], reversible two-dimensional to two-dimensional (2D-to-2D) [35,36] and zero-dimensional to one-dimensional (0D-to-1D) [37] crystal-to-crystal transformation, and irreversible structural transformation [38–40]. Herein, we have designed an imide-based O-donor ligand, 4-carboxyphenyl-1,3-dioxoisindoline-5-carboxylic acid ($H_2In\text{-}4\text{-ba}$, Scheme 1), and synthesized a high thermally stable helical chain structure, $[Zn(In\text{-}4\text{-ba})(py)_2]_n$ (**1**, py = pyridine), under hydro(solvo)thermal conditions. Noteworthy, **1** and its desolvated phase, $[Zn(In\text{-}4\text{-ba})]_n$ (**1'**), show reversible crystal-to-crystal transformations upon decoordination and recoordination of py ligands. Further, photoluminescence properties of as-synthesized, desolvated, and resolvated materials have also been studied.

* Corresponding author.

E-mail address: jyunwu@ncnu.edu.tw (J.-Y. Wu).



Scheme 1. Molecular structure of H₂In-4-ba.

2. Experimental section

2.1. Materials and instruments

Chemical reagents were purchased commercially and were used as received without further purification. ¹H NMR spectrum was recorded on a Bruker AMX-300 Solution-NMR spectrometer. All chemical shifts are reported in δ unit with reference to the residual protons of the deuterated solvent. Coupling constants are given in Hertz. Mass spectra were recorded on a JEOL JMS-700 double focusing mass spectrometer. Thermogravimetric (TG) analyses were recorded on a Thermo Cahn Versa-Therm HS TG analyzer under nitrogen atmosphere. X-ray powder diffraction (XRPD) measurements were recorded on a Shimadzu XRD-7000 diffractometer with a graphite monochromatized Cu K α radiation ($\lambda = 1.5406 \text{ \AA}$) at 40 kV and 30 mA. Infrared (IR) spectra were recorded on a Perkin-Elmer RX1 FT-IR spectrometer in the 4000–500 cm⁻¹ region using KBr discs. Solid-state excitation and emission spectra were recorded on a Hitachi F7000 fluorescence spectrophotometer at ambient temperature. CHN elemental microanalyses were performed on an Elementar Vario EL III analytical instrument.

2.2. Synthesis of 4-carboxyphenyl-1,3-dioxoisindoline-5-carboxylic acid (H₂In-4-ba)

In a round bottle, 4-aminobenzoic acid (0.69 g, 5.0 mmol) in glacial acetic acid (10 mL) was slowly added into a solution of trimellitic anhydride (0.96 g, 5.0 mmol) in glacial acetic acid (30 mL), and then the solution was heated to 180 °C with stirring for 8 h (Scheme S1). After cooling to room temperature, the solution was stirred for further 6 h and then the reaction solvents were removed under reduced pressure. The crude residue was washed with deionized water (100 mL) to give H₂In-4-ba as white powders. Yield 84% (1.32 g, 4.2 mmol). ¹H NMR (300 MHz, DMSO-*d*₆): δ 8.42 (dd, *J* = 7.5, 1.2 Hz, 1H), 8.32 (d, *J* = 0.6 Hz, 1H), 8.09 (dd, *J* = 6.8, 2.1 Hz, 3H), 7.61 (dd, *J* = 6.9, 1.8 Hz, 2H) ppm. MS (EI⁺): *m/z* 311.1 [M]⁺ (calcd for C₁₆H₉NO₆: *m/z* 311.25). Anal. calcd for C₁₆H₉NO₆: C, 61.74; H, 2.91; N, 4.50%. Found: C, 61.93; H, 3.03; N, 4.59%. IR (KBr pellet): $\bar{\nu}$ 1782, 1734, 1708, 1605, 1510, 1483, 1429, 1375, 1300, 1218, 1090, 927, 771, 724, 547 cm⁻¹.

2.3. Synthesis of [Zn(In-4-ba)(py)₂]_n (1)

H₂In-4-ba (31.1 mg, 1.0 × 10⁻¹ mmol), Zn(OAc)₂ (9.2 mg, 5.0 × 10⁻² mmol), and pyridine (py, 5 mL) were conducted in an acid digestion bomb at 90 °C for 36 h. After cooling to room temperature, the solvents were filtered off. Colorless prismatic crystals were collected in a yield of 96% (25.8 mg, 4.8 × 10⁻² mmol). Anal. calcd for C₂₆H₁₇N₃O₆Zn: C, 58.61; H, 3.22; N, 7.89%. Found: C, 59.24; H, 3.36; N, 7.81%. IR (KBr pellet): $\bar{\nu}$ 1780, 1720, 1622, 1606, 1508, 1448, 1360, 1220, 1068, 1046, 836, 780, 730, 698 cm⁻¹.

Table 1
Crystallographic data for **1**.

Empirical formula	C ₂₆ H ₁₇ N ₃ O ₆ Zn
M _w	532.79
Crystal system	Monoclinic
Space group	C2/c
a/Å	15.6419(8)
b/Å	20.7242(8)
c/Å	22.0140(16)
$\beta/^\circ$	110.727(6)
V/Å ³	6674.3(7)
Z	8
T/K	150(2)
$\lambda/\text{\AA}$	0.71073
F_{000}	3264
R ₁ , ^a wR ₂ , ^b ($I > 2\sigma(I)$)	0.0645, 0.1633
R ₁ , ^a wR ₂ , ^b (all data)	0.0969, 0.1709
GOF on F^2	1.107
$\Delta\rho_{\max}, \Delta\rho_{\min}/e \text{ \AA}^{-3}$	0.789, -0.902

^a $R_1 = \sum ||F_o| - |F_c|| / \sum |F_o|$.

^b $wR_2 = \{ \sum [w(F_o^2 - F_c^2)^2] / \sum [w(F_o^2)^2] \}^{1/2}$.

2.4. X-ray crystallography

X-ray diffraction intensity data for **1** were collected on an Oxford Diffraction Gemini S diffractometer equipped with a graphite monochromatized Mo K α radiation at 150(2) K. Starting models for structure refinement were found by direct methods using SHELXS-97 [41] and refined anisotropically on F^2 by the full-matrix least-squares technique using the SHELXL-2014/7 [42] and WINGX [43] program packages. Experimental details for X-ray data collection and the refinements are summarized in Table 1. CCDC 2060260 contains the supplementary crystallographic data for this paper. These data can be obtained free of charge from the Cambridge Crystallographic Data Centre via www.ccdc.cam.ac.uk/data_request/cif.

3. Results and discussion

3.1. Synthesis and crystal structure of [Zn(In-4-ba)(py)₂] (1)

Coordination polymer **1** was synthesized from the hydro(solvo)thermal reactions of Zn(OAc)₂ and H₂In-4-ba using pyridine (py) as solvent at 90 °C for 36 h. As a well-known fact that the hydro(solvo)thermal synthesis gives a unique combination of pressure and temperature conditions for crystallization of such products [44–47]. Single-crystal X-ray diffraction analysis reveals that **1** crystallized in the monoclinic space group C2/c. In the asymmetric unit, there are two crystallographic distinct Zn(II) centers, where Zn(1) located at a special position symmetry-related by a 2-fold rotation axis while Zn(2) located at a general position, and two crystallographic distinct In-4-ba²⁻ ligands, where one is general case with fully occupation and the other is disordered over a 2-fold rotation axis with half-occupation. For the fully-occupied In-4-ba²⁻ ligand, one of the two carboxylate groups is disordered over two statistical positions with site-of-occupancy of approximately 0.55 for O(3) and O(4) and 0.45 for O(3') and (O4'). Selected bond lengths and bond angles are listed in Table S1. In considering the coordination environments around the Zn(II) centers, Zn(1) is coordinated by two py ligands (N(3) and N(3)#1, #1 = -x, y, -z + 1/2), with a uniform Zn(1)–N bond length of 2.059(4) Å, and four carboxylate O atoms (O(3), O(4), O(3)#1, and O(4)#1, #1 = -x, y, -z + 1/2) of two In-4-ba²⁻ ligands, with the Zn(1)–O bond lengths of 1.991(8)–2.304(7) Å, to form a distorted octahedral {ZnN₂O₄} coordination geometry (or alternatively, Zn(1) is coordinated by two py ligands (N(3) and N(3)#1, #1 = -x, y, -z + 1/2), with a uniform Zn(1)–N bond

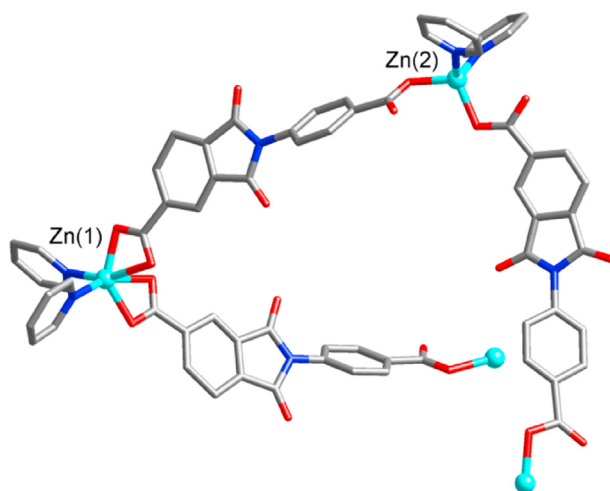


Fig. 1. The coordination environments around the two crystallographic distinct Zn(II) centers and the coordination modes of the two crystallographic distinct In-4-ba²⁻ ligands in **1**. The disordered part is omitted for clarity. Color scheme: cyan, Zn; grey, C; blue, N; red, O. (For interpretation of the references to colour in this figure legend, the reader is referred to the Web version of this article.)

length of 2.059(4) Å, and two carboxylate O atoms (O(3') and O(3')#1, #1 = -x, y, -z + 1/2) of two In-4-ba²⁻ ligands, with a uniform Zn(1)–O bond length of 2.023(9) Å, to form a distorted tetrahedral {ZnN₂O₂} coordination geometry, while Zn(2) is coordinated by two py ligands (N(4) and N(5)), with the Zn(2)–N bond lengths of 2.029(4)–2.032(4) Å, and two carboxylate O atoms (O(5) and O(9)) of two In-4-ba²⁻ ligands, with the Zn(2)–O bond lengths of 1.944(3)–1.956(4) Å, to form a distorted tetrahedral {ZnN₂O₂} coordination geometry, as shown in Fig. 1 and Fig. S4. In considering the coordination behaviors of the In-4-ba²⁻ ligands, one of the two crystallographic distinct In-4-ba²⁻ ligands, with fully occupation, bridges one Zn(1) and one Zn(2) centers with a Zn···Zn separation of 16.31 Å through the two carboxylate groups, where one is in a monodentate mode and the other is in a bidentate of asymmetric chelating mode (or alternatively, both are in a uniform monodentate mode), while the other distinct In-4-ba²⁻ ligand connects two Zn(2) centers with a Zn···Zn separation of 15.87 Å through the two carboxylate groups both in a uniform monodentate mode, as shown in Fig. 1 and Fig. S5. Connections of Zn(II) centers and In-4-ba²⁻ligands generate one-dimensional quasi-3₁ helical chain screwing in the *a* direction with a pitch of 15.64 Å (Fig. 2a). Any two neighboring helices with the same helicity are interwoven each other to lead to consecutively interweaving poly-helices along the crystallographic *b* axis in ABAB sequence, resulting

in a two-dimensional homochiral layer lying on the *ab* plane (Fig. 2b). Two neighboring homochiral layers display opposite chirality, thus individual crystal of **1** is in a racemic manner (Fig. 2c).

3.2. Thermal stability

The thermal stability of **1** was examined by thermogravimetric (TG) analysis, performed on polycrystalline samples under a nitrogen atmosphere. As shown in Fig. 3, the TG curve of **1** showed a largely unchanged until the coordinated py ligands were released between 230 and 305 °C (found, 29.1%; calcd. 29.6%). The remaining coordination framework was retained until the temperature was raised to approaching 440 °C, followed by a decomposition of the species. The final decomposition product was reasonably assigned to ZnO (found, 15.3%; calcd. 15.0%). The TG analysis implies that **1** shows high thermal stability.

3.3. Reversible crystal-to-crystal transformations

X-ray powder diffraction (XRPD) analysis indicated that the experimental and simulated diffraction patterns of **1** are closely matched, implying that the bulky materials are formed in a high purity of single phase (Fig. 4a). On heating a crystalline sample of **1** at a temperature of 300 °C for 1 h gave a desolvated phase, [Zn(In-4-ba)]_n (**1'**). It is noted that the desolvated phase **1'** retained the visual crystal morphology but lost the transparency of the crystals (Fig. 4b), so that its single-crystal character became very poor for single-crystal X-ray diffraction analysis.

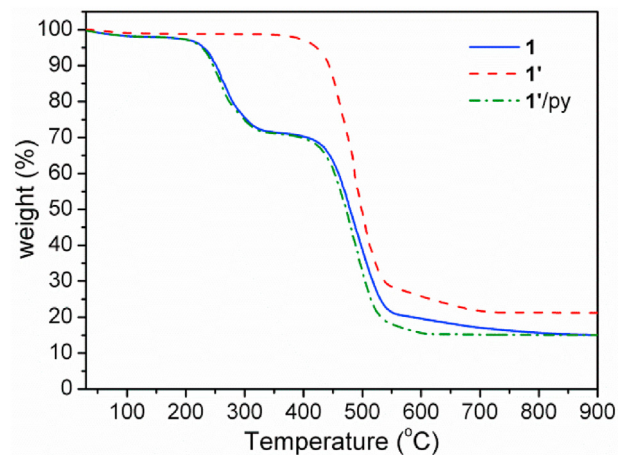


Fig. 3. TG curves of as-synthesized **1**, desolvated **1'**, and resolvated **1'/py**.

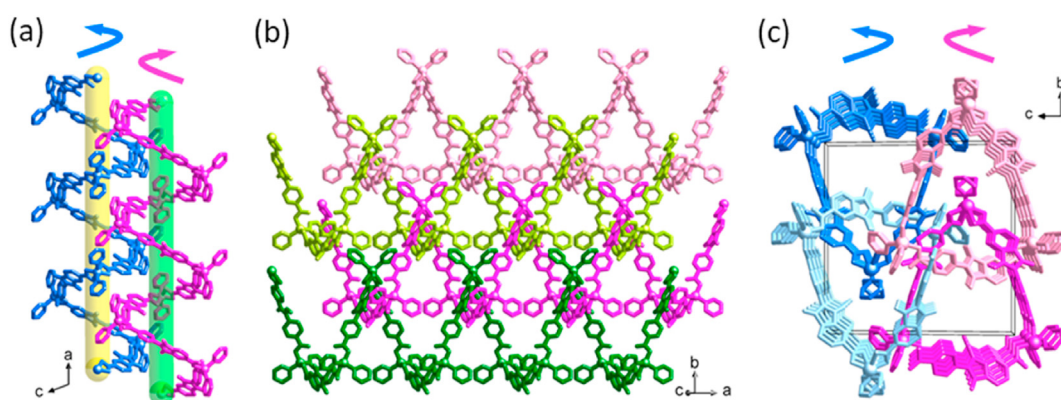


Fig. 2. Representations of (a) the one-dimensional right-handed (blue) and left-handed (pink) quasi-3₁ helical chains, (b) the homochiral layer of consecutively interweaving left-handed poly-helices in ABAB order along the *b* axis, and (c) the racemic packing arrangement of homochiral layers with opposite chirality in individual crystal of **1**. Color scheme: blue and pale-blue: right-handed helical chains; pink and pale-pink: left-handed helical chains. (For interpretation of the references to colour in this figure legend, the reader is referred to the Web version of this article.)

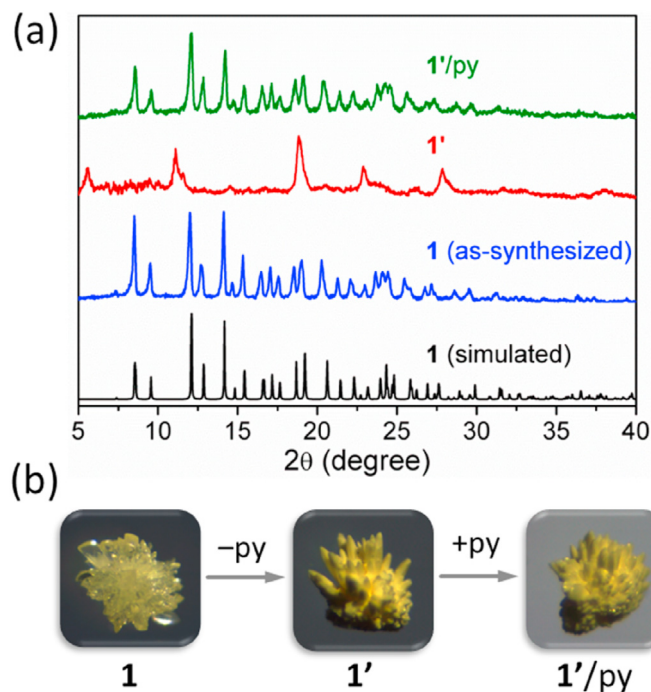


Fig. 4. (a) XRPD patterns of simulated and as-synthesized **1**, desolvated **1'**, and resolvated **1'/py**. (b) Photographs of crystals for the reversible crystal-to-crystal transformations of solvated **1** to desolvated **1'** and back to solvated **1**.

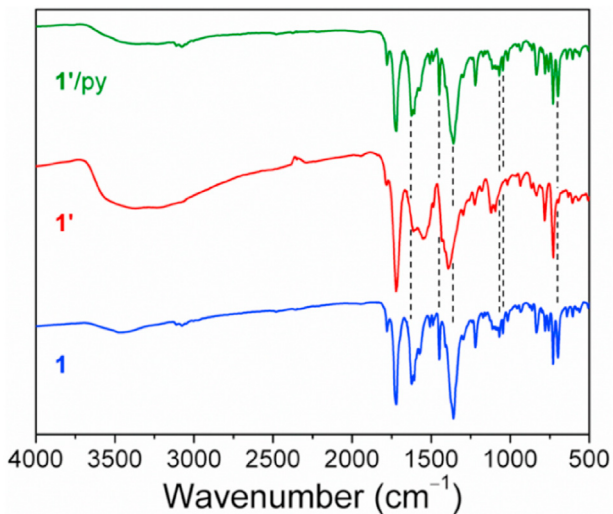


Fig. 5. IR spectra of as-synthesized **1**, desolvated **1'**, and resolvated **1'/py**.

However, the XRPD patterns of **1'** showed broadened peaks that are different from the simulated and as-synthesized ones (Fig. 4a), resulting in phase conversion to form a new crystalline phase in poor crystallinity, might be due to desolvation-induced framework distortion or structure reorganization. Of particular interest, when desolvated phase **1'** was allowed to immerse in py solvent at room temperature for 1 day, the so-obtained solids, **1'/py**, showed the recovery of diffraction peaks (Fig. 4a), compared to the XRPD patterns of simulated and as-synthesized **1**. This confirms the regeneration of solvated **1** very well, even though the single-crystal character is not good enough (Fig. 4b). As a result, reversible crystal-to-crystal transformations between solvated **1** and desolvated **1'** have been achieved upon reversible decoordination and recoordination of py ligands. In particular, the single crystals keep morphology instead of collapse in this process (Fig. 4b).

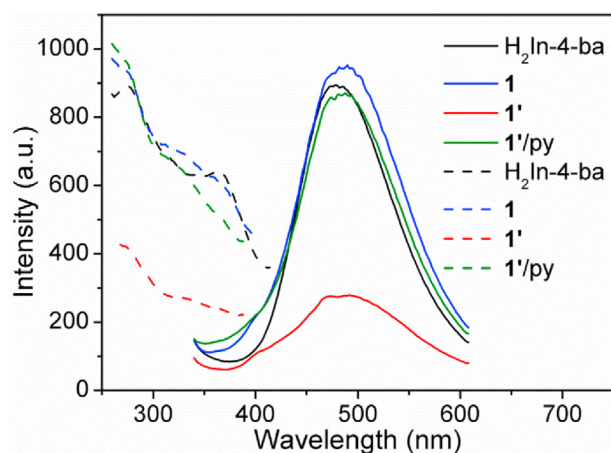


Fig. 6. Solid-state fluorescence excitation (dashed lines) and emission (solid lines) spectra of **H₂In-4-ba**, as-synthesized **1**, desolvated **1'**, and resolvated **1'/py** at room temperature. The wavelength of emission monochromator is set to be 450 nm for **H₂In-4-ba**, **1**, and **1'/py** and 500 nm for **1'** for excitation spectra. The wavelength of excitation monochromator is set to be 320 nm for **H₂In-4-ba**, **1**, and **1'/py** for emission spectra.

On the other hand, TG curve of desolvated **1'** shows a large of flat before framework collapse at about 440 °C, as shown in Fig. 3. After immersing **1'** in py solvent, the recovered solids, **1'/py**, showed similar TG trace as that of as-synthesized **1**. In addition, IR spectra show dramatic changes after desolvation. As shown in Fig. 5, the vibrations at 1360 and 1606 cm⁻¹ for **1** are respectively blue-shifted to 1692 and 1614 cm⁻¹ for **1'** whereas the vibrations at 1622, 1448, 1068, 1046, and 698 cm⁻¹ are disappeared. In addition, the vibrations in the region of 1662–1458 cm⁻¹ are apparently broadened for **1'**. These changes, however, would be completely returned back after resolvation of **1'**. Therefore, TG analysis and IR spectra provide further supports for the reversible crystal-to-crystal transformations between solvated **1** and desolvated **1'**.

To the best of our knowledge, reversible crystal-to-crystal transformations are relatively rare for one-dimensional coordination polymers [29,34,37,48], compared to that for two- and three-dimensional frameworks. The recoverable transformation characteristics induced by desolvation and resolvation make **1** to be a potential solvent carrier [19–23, 34,35].

3.4. Photoluminescence properties

Photoluminescence properties of the free **H₂In-4-ba** and **1** were investigated in solid-state at room temperature (Fig. 6). The free ligand exhibits an emission band centered at 486 nm ($\lambda_{\text{ex}} = 320 \text{ nm}$), reasonably assigned to the ligand-centered $\pi^* \rightarrow \pi$ and/or $n \rightarrow \pi$ transitions. Compared to the free **H₂In-4-ba**, the emission band of **1** are slightly blue-shifted to 482 nm ($\lambda_{\text{ex}} = 320 \text{ nm}$), which is tentatively assigned to originate from the ligand-centered charge transfer from the band shape and position. Upon thermal activation, desolvated **1'** exhibits an emission band centered at 492 nm ($\lambda_{\text{ex}} = 320 \text{ nm}$), which is largely weakened in the intensity, suggesting the effect of coordinated py ligands and/or structure regulation [34,49,50]. After resolvation in py solvent, resolvated **1'/py** shows emission spectrum very similar to that of as-synthesized **1**, confirming again the recovery of **1**.

4. Conclusion

In this work, a luminescent zinc(II) coordination polymer **1** showing high thermal stability with a temperature approaching 440 °C and ligand-centered solid-state emission with a maximum at 486 nm has been hydro(solvothermally synthesized and structurally characterized. Coordination polymer **1** has a quasi-3₁ helical chain structure obtained from

achiral components; these helical chains with the same helicity interweave each other consecutively, resulting in a homochiral layer and thus causing $1D \rightarrow 2D$ dimensionality extension. Noteworthy, individual crystal of **1** is racemic instead of conglomerate as a result of the coexistence of homochiral layers of opposite chirality in equal amounts. The obtained compound broadens an increasing family of luminescent zinc(II) coordination polymers [3–6]. Moreover, XRPD patterns, IR spectra, TG diagrams, and photoluminescence spectra have evidenced that the solvated **1** and desolvated **1'** would process reversible crystal-to-crystal transformation induced by decoordination and recoordination of py ligands. This phenomenon make **1** potential candidate to be applied as a solvent carrier.

Author statement

All persons who meet authorship criteria are listed as authors, and all authors certify that they have participated sufficiently in this work, and take public responsibility for the content, including participation in the concept, experiment design, data analysis, writing as well as revision of the manuscript. All authors agree the corresponding author (Jing-Yun Wu) as the representative person for handling this manuscript.

CRediT authorship contribution statement

Chung-Yu Chang: Investigation, Data curation. **Meng-Jung Tsai:** Investigation, Data curation. **Jing-Yun Wu:** Conceptualization, Resources, Data curation, Writing – original draft, Writing – review & editing.

Declaration of competing interest

The authors declare that they have no known competing financial interests or personal relationships that could have appeared to influence the work reported in this paper.

Acknowledgments

We gratefully acknowledge the National Chi Nan University and the Ministry of Science and Technology of Taiwan (NSC 98-2113-M-260-004-MY2, NSC 100-2113-M-260-003-MY2, and MOST 108-2113-M-260-002-) for the financial support. We thank the Instrument Center at National Chung Hsing University for providing valuable assistance on Elemental Analysis and Single Crystal X-Ray Diffractometer.

Appendix A. Supplementary data

Supplementary data to this article can be found online at <https://doi.org/10.1016/j.jssc.2021.122129>.

References

- [1] H. Li, K. Wang, Y. Sun, C.T. Lollar, J. Li, H.-C. Zhou, Recent advances in gas storage and separation using metal–organic frameworks, *Mater. Today* 21 (2018) 108–121.
- [2] L. Zhu, X.-Q. Liu, H.-L. Jiang, L.-B. Sun, Metal–Organic frameworks for heterogeneous basic catalysis, *Chem. Rev.* 117 (2017) 8129–8176.
- [3] W.P. Lustig, S. Mukherjee, N.D. Rudd, A.V. Desai, J. Li, S.K. Ghosh, Metal–organic frameworks: functional luminescent and photonic materials for sensing applications, *Chem. Soc. Rev.* 46 (2017) 3242–3285.
- [4] W. Huang, F. Pan, Y. Liu, S. Huang, Y. Li, J. Yong, Y. Li, A.M. Kirillov, D. Wu, An efficient blue-emissive Metal–Organic Framework (MOF) for lanthanide-encapsulated multicolor and stimuli-responsive luminescence, *Inorg. Chem.* 56 (2017) 6362–6370.
- [5] R.-X. Yao, X. Cui, X.-X. Jia, F.-Q. Zhang, X.-M. Zhang, A luminescent zinc(II) Metal–Organic Framework (MOF) with conjugated π -electron ligand for high iodine capture and nitro-explosive detection, *Inorg. Chem.* 55 (2016) 9270–9275.
- [6] L. Qiu, C. Yu, X. Wang, Y. Xie, A.M. Kirillov, W. Huang, J. Li, P. Gao, T. Wu, X. Gu, Q. Nie, D. Wu, Tuning the solid-state white light emission of postsynthetic lanthanide-encapsulated double-layer MOFs for three-color luminescent thermometry applications, *Inorg. Chem.* 58 (2019) 4524–4533.
- [7] K. Wang, Q. Li, Z. Ren, C. Li, Y. Chu, Z. Wang, M. Zhang, H. Wu, Q. Zhang, 2D Metal–Organic Frameworks (MOFs) for high-performance BatCap hybrid devices, *Small* 16 (2020) 2001987.
- [8] K.-B. Wang, Q. Xun, Q. Zhang, Recent progress in metal–organic frameworks as active materials for supercapacitors, *EnergyChem* 2 (2020) 100025.
- [9] K. Wang, B. Lv, Z. Wang, H. Wu, J. Xu, Q. Zhang, Two-fold interpenetrated Mn-based metal–organic frameworks (MOFs) as battery-type electrode materials for charge storage, *Dalton Trans.* 49 (2020) 411–417.
- [10] K. Wang, R. Bi, M. Huang, B. Lv, H. Wang, C. Li, H. Wu, Q. Zhang, Porous cobalt Metal–Organic frameworks as active elements in Battery–Supercapacitor hybrid devices, *Inorg. Chem.* 59 (2020) 6808–6814.
- [11] K. Wang, Z. Wang, J. Liu, C. Li, F. Mao, H. Wu, Q. Zhang, Enhancing the performance of a Battery–Supercapacitor hybrid energy device through narrowing the capacitance difference between two electrodes via the utilization of 2D MOF-nanosheet-derived Ni@Nitrogen-Doped-Carbon Core–Shell rings as both negative and positive electrodes, *ACS Appl. Mater. Interfaces* 12 (2020), 47482–47489.
- [12] Y. Yan, C. Li, Y. Wu, J. Gao, Q. Zhang, From isolated Ti-oxo clusters to infinite Ti-oxo chains and sheets: recent advances in photoactive Ti-based MOFs, *J. Mater. Chem. A* 8 (2020) 15245–15270.
- [13] Y. Li, M. Lu, Y. Wu, Q. Ji, H. Xu, J. Gao, G. Qian, Q. Zhang, Morphology regulation of metal–organic framework-derived nanostructures for efficient oxygen evolution electrocatalysis, *J. Mater. Chem. A* 8 (2020) 18215–18219.
- [14] Y. Li, T. Zhao, M. Lu, Y. Wu, Y. Xie, H. Xu, J. Gao, J. Yao, G. Qian, Q. Zhang, Enhancing oxygen evolution reaction through modulating electronic structure of trimetallic electrocatalysts derived from Metal–Organic frameworks, *Small* 15 (2019) 1901940.
- [15] J.-P. Zhang, P.-Q. Liao, H.-L. Zhou, R.-B. Lin, X.-M. Chen, Single-crystal X-ray diffraction studies on structural transformations of porous coordination polymers, *Chem. Soc. Rev.* 43 (2014) 5789–5814.
- [16] G.K. Kole, J.J. Vittal, Solid-state reactivity and structural transformations involving coordination polymers, *Chem. Soc. Rev.* 42 (2013) 1755–1775.
- [17] C.-P. Li, J. Chen, C.-S. Liu, M. Du, Dynamic structural transformations of coordination supramolecular systems upon exogenous stimulation, *Chem. Commun.* 51 (2015) 2768–2781.
- [18] B. Manna, A.V. Desai, S.K. Ghosh, Neutral N-donor ligand based flexible metal–organic frameworks, *Dalton Trans.* 45 (2016) 4060–4072.
- [19] M. Shivanna, Q.-Y. Yang, A. Bajpai, E. Patyk-Kazmierczak, M.J. Zaworotko, A dynamic and multi-responsive porous flexible metal–organic material, *Nat. Commun.* 9 (2018) 3080.
- [20] Y.-L. Lu, J.-Y. Wu, M.-C. Chan, S.-M. Huang, C.-S. Lin, T.-W. Chiu, Y.-H. Liu, Y.-S. Wen, C.-H. Ueng, T.-M. Chin, C.-H. Hung, K.-L. Lu, Influence of water content on the self-assembly of Metal–Organic frameworks based on pyridine-3,5-dicarboxylate, *Inorg. Chem.* 45 (2006) 2430–2437.
- [21] C.-B. Tian, R.-P. Chen, C. He, W.-J. Li, Q. Wei, X.-D. Zhang, S.-W. Du, Reversible crystal-to-amorphous-to-crystal phase transition and a large magnetocaloric effect in a sponge-like metal organic framework material, *Chem. Commun.* 50 (2014) 1915–1917.
- [22] K.S. Lim, J.H. Song, D.W. Kang, M. Kang, S. Eom, E.K. Koh, C.S. Hong, Reversible crystal-to-amorphous structural transformations and magnetic variations in single end-on azide-bridged M^{II} ($M = \text{Mn, Ni}$) coordination polymers, *Dalton Trans.* 47 (2018) 845–851.
- [23] M.-H. Zeng, Y.-X. Tan, Y.-P. He, Z. Yin, Q. Chen, M. Kurmoo, A porous 4-fold-interpenetrated chiral framework exhibiting vapochromism, single-crystal-to-single-crystal solvent exchange, gas sorption, and a poisoning effect, *Inorg. Chem.* 52 (2013) 2353–2360.
- [24] T.-Y. Ho, S.-M. Huang, J.-Y. Wu, K.-C. Hsu, K.-L. Lu, Direct guest exchange induced single-crystal to single-crystal transformation accompanying irreversible crystal expansion in soft porous coordination polymers, *Cryst. Growth Des.* 15 (2015) 4266–4271.
- [25] T.K. Pal, D. De, S. Neogi, P.K. Bharadwaj, Guest dependent reversible single-crystal to single-crystal structural transformation in a flexible Gd(iii)-coordination polymer, *Inorg. Chem. Front.* 2 (2015) 395–402.
- [26] G. Mukherjee, K. Biradha, Post-synthetic modification of isomorphic coordination layers: exchange dynamics of metal ions in a single crystal to single crystal fashion, *Chem. Commun.* 48 (2012) 4293–4295.
- [27] J. Tian, L.V. Saraf, B. Schwenzer, S.M. Taylor, E.K. Brechin, J. Liu, S.J. Dalgarno, P.K. Thallapally, Selective metal cation capture by soft anionic metal–organic frameworks via drastic single-crystal-to-single-crystal transformations, *J. Am. Chem. Soc.* 134 (2012) 9581–9584.
- [28] L. Hashemi, A. Morsali, O. Büyükgüngör, Anion influence on transformations of a nonporous 3D to porous 3D coordination polymer, *New J. Chem.* 38 (2014) 3187–3192.
- [29] B.-C. Tzeng, T.-Y. Chang, H.-S. Sheu, Reversible phase transformation and luminescent mechanochromism of Zn^{II} -based coordination frameworks containing a dipyridylamide ligand, *Chem. Eur. J.* 16 (2010) 9990–9993.
- [30] M. Wang, X. Meng, F. Song, Y. He, W. Shi, H. Gao, J. Tang, C. Peng, Reversible structural transformation induced switchable single-molecule magnet behavior in lanthanide metal–organic frameworks, *Chem. Commun.* 54 (2018) 10183–10186.
- [31] I.-H. Park, R. Medishetty, J.-Y. Kim, S.S. Lee, J.J. Vittal, Distortional supramolecular isomers of polyrotaxane coordination polymers: photoreactivity and sensing of nitro compounds, *Angew. Chem. Int. Ed.* 53 (2014) 5591–5595.
- [32] Y.C. Ou, D.S. Zhi, W.T. Liu, Z.P. Ni, M.L. Tong, Single-Crystal-to-Single-Crystal transformation from 1D staggered-sculls chains to 3D NbO-type Metal–Organic framework through [2+2] photodimerization, *Chem. Eur. J.* 18 (2012), 7357–7361.

- [33] V. Safarifard, A. Morsali, Mechanochemical solid-state transformations from a 3D lead(II) chloride triazole carboxylate coordination polymer to its bromide/thiocyanate analogs via anion-replacements: precursors for the preparation of lead(II) chloride/bromide/sulfide nanoparticles, *CrystEngComm* 14 (2012) 5130–5132.
- [34] J.-Y. Wu, C.-Y. Chang, C.-J. Tsai, J.-J. Lee, Reversible single-crystal to single-crystal transformations of a Zn(II)–Salicyaldimine coordination polymer accompanying changes in coordination sphere and network dimensionality upon dehydration and rehydration, *Inorg. Chem.* 54 (2015) 10918–10924.
- [35] J.-R. Zhang, J.-J. Lee, C.-H. Su, M.-J. Tsai, C.-Y. Li, J.-Y. Wu, From lamellar net to bilayered-lamella and to porous pillared-bilayer: reversible crystal-to-crystal transformation, CO₂ adsorption, and fluorescence detection of Fe³⁺, Al³⁺, Cr³⁺, MnO₄⁻, and Cr₂O₇²⁻ in water, *Dalton Trans.* 49 (2020) 14201–14215.
- [36] Y.-W. Huang, P.-M. Chuang, J.-Y. Wu, Solvent-induced controllable supramolecular isomerism: phase transformation, CO₂ adsorption, and fluorescence sensing toward CrO₄²⁻, Cr₂O₇²⁻, MnO₄⁻ and Fe³⁺, *Inorg. Chem.* 59 (2020) 9095–9107.
- [37] Y.-J. Tseng, J.-Y. Wu, Reversible structural transformations between a chain polymer and a metalloccage induced by anion templation, *Inorg. Chim. Acta* 455 (2017) 241–246.
- [38] M.-J. Tsai, C.-Y. Li, J.-Y. Wu, A highly stable luminescent coordination polymer for sensing of volatile iodine and its metal-ion exchange properties with Cu²⁺ ions, *J. Photochem. Photobiol. A: Chem.* 389 (2020) 112256.
- [39] J.-Y. Wu, C.-J. Tsai, C.-Y. Chang, Y.-Y. Wu, Metal-ion exchange induced structural transformation as a way of forming novel Ni(II)– and Cu(II)–salicyaldimine structures, *J. Solid State Chem.* 246 (2017) 23–28.
- [40] J.-Y. Wu, Y.-C. Liu, T.-C. Chao, From 1D helix to 0D loop: nitrite anion induced structural transformation associated with unexpected N-nitrosation of amine ligand, *Inorg. Chem.* 53 (2014) 5581–5588.
- [41] G.M. Sheldrick, A short history of SHELX, *Acta Crystallogr. A* 64 (2008) 112–122.
- [42] G.M. Sheldrick, Crystal structure refinement with SHELXL, *Acta Crystallogr. C* 71 (2015) 3–8.
- [43] L.J. Farrugia, WinGX and ORTEP for windows: an update, *J. Appl. Crystallogr.* 45 (2012) 849–854.
- [44] Y. Zhao, K. Li, J. Li, Solvothermal synthesis of multifunctional coordination polymers, *Z. Naturforsch.* 65b (2010) 976–998.
- [45] S. Sanati, R. Abazari, A. Morsali, A.M. Kirillov, P.C. Junk, J. Wang, An asymmetric supercapacitor based on a non-calcined 3D pillared cobalt(II) Metal–Organic framework with long cyclic stability, *Inorg. Chem.* 58 (2019) 16100–16111.
- [46] W. Huang, J. Jiang, D. Wu, B. Xue, A.M. Kirillov, A highly stable nanotubular MOF rotator for selective adsorption of benzene and separation of xylene isomers, *Inorg. Chem.* 54 (2015) 10524–10526.
- [47] J.-Z. Gu, X.-X. Liang, Y. Cai, J. Wu, Z.-F. Shi, A.M. Kirillov, Hydrothermal assembly, structures, topologies, luminescence, and magnetism of a novel series of coordination polymers driven by a trifunctional nicotinic acid building block, *Dalton Trans.* 46 (2017) 10908–10925.
- [48] A. Aslani, A. Morsali, Crystal-to-crystal transformation from a chain polymer to a two-dimensional network by thermal desolvation, *Chem. Commun.* (2008) 3402–3404.
- [49] Y. Wu, X. Zhang, L.-J. Xu, M. Yang, Z.-N. Chen, Luminescent vapochromism due to a change of the ligand field in a one-dimensional manganese(II) coordination polymer, *Inorg. Chem.* 57 (2018) 9175–9181.
- [50] W. Gao, M. Leng, Z. Hu, J. Li, D. Li, H. Liu, L. Gao, G. Niu, J. Tang, Reversible luminescent humidity chromism of organic–inorganic hybrid PEA 2 MnBr 4 single crystals, *Dalton Trans.* 49 (2020) 5662–5668.